ORIGINAL ARTICLE

Individual variation in longitudinal postnatal development of the primate brain

G. Ball[1] · M. L. Seal[1,2]

Abstract
Quantifying individual variation in postnatal brain development can provide insight into cognitive diversity within a population and the aetiology of common neuropsychiatric and neurodevelopmental disorders. Non-invasive studies of the non-human primate can aid understanding of human brain development, facilitating longitudinal analysis during early postnatal development when comparative human populations are difficult to sample. In this study, we perform analysis of a longitudinal MRI dataset of 32 macaques, each with up to five magnetic resonance imaging (MRI) scans acquired between 3 and 36 months of age. Using nonlinear mixed effects model we derive growth trajectories for whole brain, cortical and subcortical grey matter, cerebral white matter and cerebellar volume. We then test the association between individual variation in postnatal tissue volumes and birth weight. We report nonlinear growth models for all tissue compartments, as well as significant variation in total intracranial volume between individuals. We also demonstrate that regional subcortical grey matter varies both in total volume and rate of change between individuals and is associated with differences in birth weight. This supports evidence that birth weight may act as a marker of subsequent brain development and highlights the importance of longitudinal MRI analysis in developmental studies.

Keywords Brain development · Macaque · Magnetic resonance imaging · Nonlinear models

Introduction

Characterising individual variation in early brain development is critical to understanding the emergence of cognitive and behavioural diversity within populations and may provide insight into the aetiology of common neuropsychiatric and neurodevelopmental disorders (Foulkes and Blakemore 2018; Seghier and Price 2018). Longitudinal data are essential to the valid estimation of individual differences (Rogosa

✉ G. Ball
  gareth.ball@mcri.edu.au

  M. L. Seal
  marc.seal@mcri.edu.au

1 Developmental Imaging, Murdoch Children's Research Institute, Melbourne, Australia

2 Department of Paediatrics, University of Melbourne, Melbourne, Australia

et al. 1982; Cudeck 1996; Kanai and Rees 2011; Madhyastha et al. 2017). Longitudinal studies of brain growth using magnetic resonance imaging (MRI) in childhood have revealed several key characteristics common across samples (Giedd et al. 1999; Gilmore et al. 2012; Mills et al. 2016). Brain growth is at its most rapid in the first year of life, and accompanied by nonlinear changes to the distributions of cortical and subcortical grey matter and cerebral white matter volume that continue through childhood and adolescence (Tamnes et al. 2010, 2017; Lebel and Beaulieu 2011; Gilmore et al. 2012; Aubert-Broche et al. 2013; Holland et al. 2014; Raznahan et al. 2014; Wierenga et al. 2014). Increasing evidence suggests that neurodevelopmental variation in youth is partly mediated by interruption to developmental processes in early life that can have a long-standing impact on cerebral development and cognitive function (Morsing et al. 2011; Raznahan et al. 2012; Walhovd et al. 2012; Sucksdorff et al. 2015; Ball et al. 2017). Alterations to typical trajectories of brain development are implicated in neurodevelopmental disorders such as autism spectrum disorder, attention-deficit hyperactivity disorder and schizophrenia and may be rooted in early life (Courchesne et al. 2003;

Douaud et al. 2009; Morsing et al. 2011; Lampi et al. 2012; Chiapponi et al. 2013; Hazlett et al. 2017). It is therefore vital to understand how the brain development varies over time within individuals, and how early disturbances to foundational processes may impact this trajectory.

Both human and non-human primates undergo a protracted period of postnatal cerebral development, characterised by rapidly increasing cerebral volume, expansion of higher-order neocortical areas and axonal myelination that coincide with dynamic alterations in gene expression (Bourgeois et al. 1994; Kinney et al. 1988; Amlien et al. 2016; Bakken et al. 2016). Across mammalian species, the relative timing of key neurodevelopmental events including neurogenesis, synaptogenesis and pruning, postnatal myelination, and brain growth are relatively conserved (Workman et al. 2013), and the relationship between brain size and body size are largely governed by allometric scaling laws across both ontogeny and phylogeny (Passingham 1985; Harvey and Pagel 1988). Despite this, several features unique to the primate brain development have been identified, including expanded cellular proliferation during neurogenesis (Smart et al. 2002) and increased cortical neuronal density for a given brain size (Herculano-Houzel et al. 2014). Non-invasive studies of the non-human primate brain with magnetic resonance imaging (MRI) can provide useful insight into human brain development, facilitating longitudinal analysis and cross-species comparison, particularly during early postnatal development when comparative human populations are difficult to sample (Hunsaker et al. 2014; Scott et al. 2016; Grootel et al. 2017; Sakai et al. 2017).

As with humans, longitudinal MRI analyses in macaques have found that total brain volume approaches two-thirds of full adult volume by 1 week of age, and follows a nonlinear trajectory over time with an initial rapid growth rate that slows from around 4 months onwards (Malkova et al. 2006; Payne et al. 2010; Scott et asl. 2016). In both species, total brain volume is, on average, larger in males, and postnatal growth is largest in frontal, parietal and temporal lobes with similar trajectories in subcortical and cerebellar volumes (Gilmore et al. 2012; Scott et al. 2016). In humans, longitudinal analyses of structural MRI have found that cortical grey matter volume doubles in the first year of life and peaks in early childhood, then gradually decreases during adolescence; white matter, on the other hand, follows a more stable trajectory with age (Gilmore et al. 2012; Mills et al. 2016). Using manual tissue segmentation, Malkova et al. found that white matter volume undergoes rapid increase up to 5 months, followed by a period of relatively stable linear growth until 4 years of age (Malkova et al. 2006). In macaques, longitudinal analyses of postnatal cortical grey matter volume are lacking, however in a cross-sectional study of 37 juvenile macaques, Knickmeyer et al. reported linear and quadratic increases of total brain volume and white matter volume, respectively, but no significant age-related change in cortical grey matter (Knickmeyer et al. 2010).

Despite relative concordance between sites and studies on the typical growth trajectory of primate brain development, open questions remains on how best to define brain tissue volume change over time—i.e. is the observed trend linear, quadratic, or cubic with age? Nonlinear growth implies periods of accelerated growth that may represent critical developmental periods or windows of vulnerability to injury. In humans, several studies have reported developmental peaks in cortical grey matter volume thought to define important points of inflection in brain development that vary meaningfully between sexes and across clinical cohorts (Sowell et al. 2004; Lenroot et al. 2007; Shaw et al. 2007; Raznahan et al. 2011; Alexander-Bloch et al. 2014). Similar observations have been made for subcortical grey matter and cerebellar volume (Raznahan et al. 2014; Wierenga et al. 2014). However, the choice of functional form can alter when, and if, peaks are defined, and the best-fit model can be dependent on the sampled population, image preprocessing strategies, model selection strategy or study design (Mills and Tamnes 2014; King et al. 2017; Walhovd et al. 2017).

Generalised additive models (GAMs) offer an alternative approach to polynomial modelling for nonlinear trends (Hastie and Tibshirani 1986). In GAMs, linear predictors are replaced by smooth functions, with the degree of smoothness estimated during model fitting (Wood 2011). As such, GAMs offer an efficient and flexible non-parametric alternative to linear models that do not require the specification of a functional form (quadratic, cubic, etc.) for the relationship between tissue volume and age (Gennatas et al. 2017; Herting et al. 2018).

In this study, we use GAMs to examine trajectories of postnatal brain development in the macaque. Using data from an open-source, neurodevelopmental macaque database (Young et al. 2017), we extend upon previous reports and model nonlinear growth of cortical grey matter, white matter, subcortical grey matter and the cerebellum. We quantify both group averaged trajectories and the individual variation present within the sample and report associations between birth weight and postnatal tissue volume.

Methods

Data

Longitudinal MRI data were acquired from the UNC-Wisconsin Rhesus Macaque Neurodevelopment Database (Young et al. 2017). This publicly available database contains MRI scans from 34 rhesus macaques (*Macaca mulatta*) housed at the Harlow Primate Laboratory (HPL)

at the University of Wisconsin-Madison and scanned up to five times between the ages of 2 weeks and 36 months. The research protocol was approved by the local Institutional Animal Care and Use Committee. Data are available to download from: https://data.kitware.com/#collection/54b582c38d777f4362aa9cb3. Full study protocols are detailed in Young et al. (2017).

After quality control and image processing (see below), 15 scans were excluded, resulting in a final dataset comprising 32 macaques (18 male) with between 2 and 5 scans (median number of scans = 5, mean = 4.5) and scanned between 3 and 36 months (mean age at scan = 13.8 months) (Fig. 1).

Neuroimaging

MRI scans were performed on a 3T scanner (General Electric Medical, Milwaukee WI) using a human eight-channel brain array coil at the University of Wisconsin-Madison. High-resolution 3D T1-weighted imaging was performed using the following parameters: TI = 450 ms, TR = 8.684 ms, TE = 3.652 ms, FOV = 140 × 140 mm, flip angle = 12°, matrix = 256 × 256, thickness = 0.8 mm, gap = − 0.4 mm,
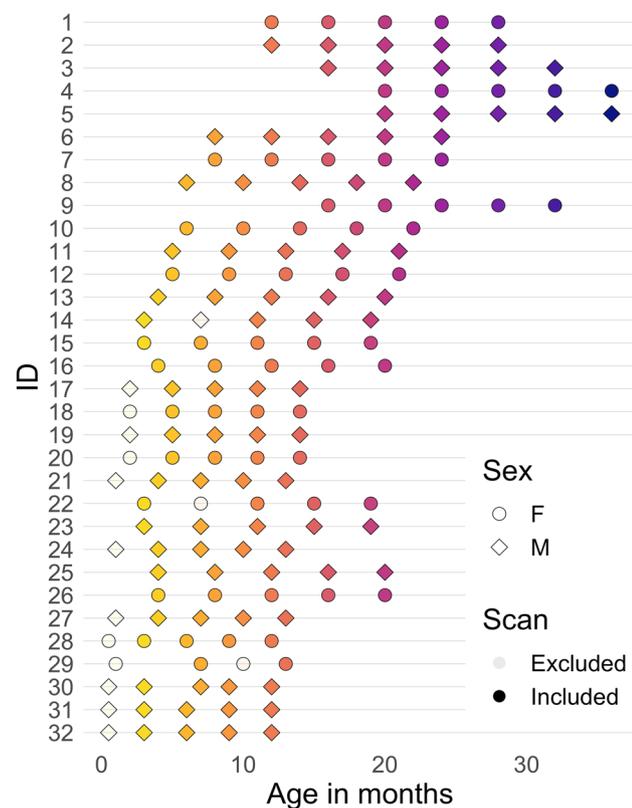

Fig. 1 Longitudinal MRI scanning schedule. Up to five MRI scans were acquired from each macaque. Plot shows the age at scan for each macaque (ID). Colour indicates age, transparency indicates timepoints excluded from the analysis, sex is shown by shape

total time = 10:46 min, providing an effective voxel resolution of 0.55 × 0.55 × 0.8 mm. As part of the scanning protocol, T2-weighted scans and 120-direction diffusion-weighted scans were also acquired (Young et al. 2017). Macaques were anaesthetised for the duration of the scan.

Image processing

The image processing pipeline is shown in Fig. 2. Raw T1 images were initially denoised using a non-local means filter (Manjón et al. 2012) and aligned using a rigid registration to the NIMH Macaque Template (NMT) (Seidlitz et al. 2018).

To perform brain extraction, T1-weighted MRI were corrected for bias field inhomogeneities and aligned to the template image using a diffeomorphic nonlinear registration in *ANTs* (Avants et al. 2008, 2011a; Tustison et al. 2010). Images were brain extracted using a probabilistic tissue segmentation (*Atropos* in *ANTs;* Avants et al. 2011b) initialised by the NMT tissue priors. Brain masks were visually checked and edited where necessary to ensure non-brain tissue was removed from individual brain masks.

To account for the longitudinal structure of the dataset, single subject templates (SST) were constructed by iterative nonlinear alignment and averaging of all available timepoints for a given subject (Avants et al. 2011a; Reuter et al. 2012), resulting in 32 SST (Fig. 2a). Nonlinear transformations were calculated between each subject's individual timepoints and the corresponding SST, and between each SST and the NMT. Each SST was segmented into three tissue classes grey matter: GM; white matter: WM, and cerebrospinal fluid (CSF) with *Atropos* using the spatial tissue priors of the NMT. Individual tissue priors were created by smoothing the SST tissue segmentations and used to initialise tissue segmentation of each individual's timepoint image (Fig. 2b).

Subcortical and allocortical structures were labelled using regional tissue labels derived from the Center for In Vivo Microscopy (CIVM) macaque atlas, consisting of 242 regional parcels hierarchically organised according to the developmental ontology of the mammalian brain (Puelles et al. 2013; Calabrese et al. 2015). Labels were combined hierarchically into a subcortical and allocortical grey matter mask (comprising the thalamus, pallidum, striatum, amygdala and hippocampus) and a cerebellar mask. Regional masks were then propagated to individual scans via the concatenated warps computed between the NMT and individual SSTs (Fig. 2a), and between each SST and each individual timepoint. Voxels contained by each mask, but not classified as CSF, were classified as subcortical or cerebellar voxels, respectively. This resulted in WM, GM, subcortical GM and cerebellar masks for each T1 image (Fig. 2b).

A visual quality check was performed for all images, with gross misclassification errors edited manually where
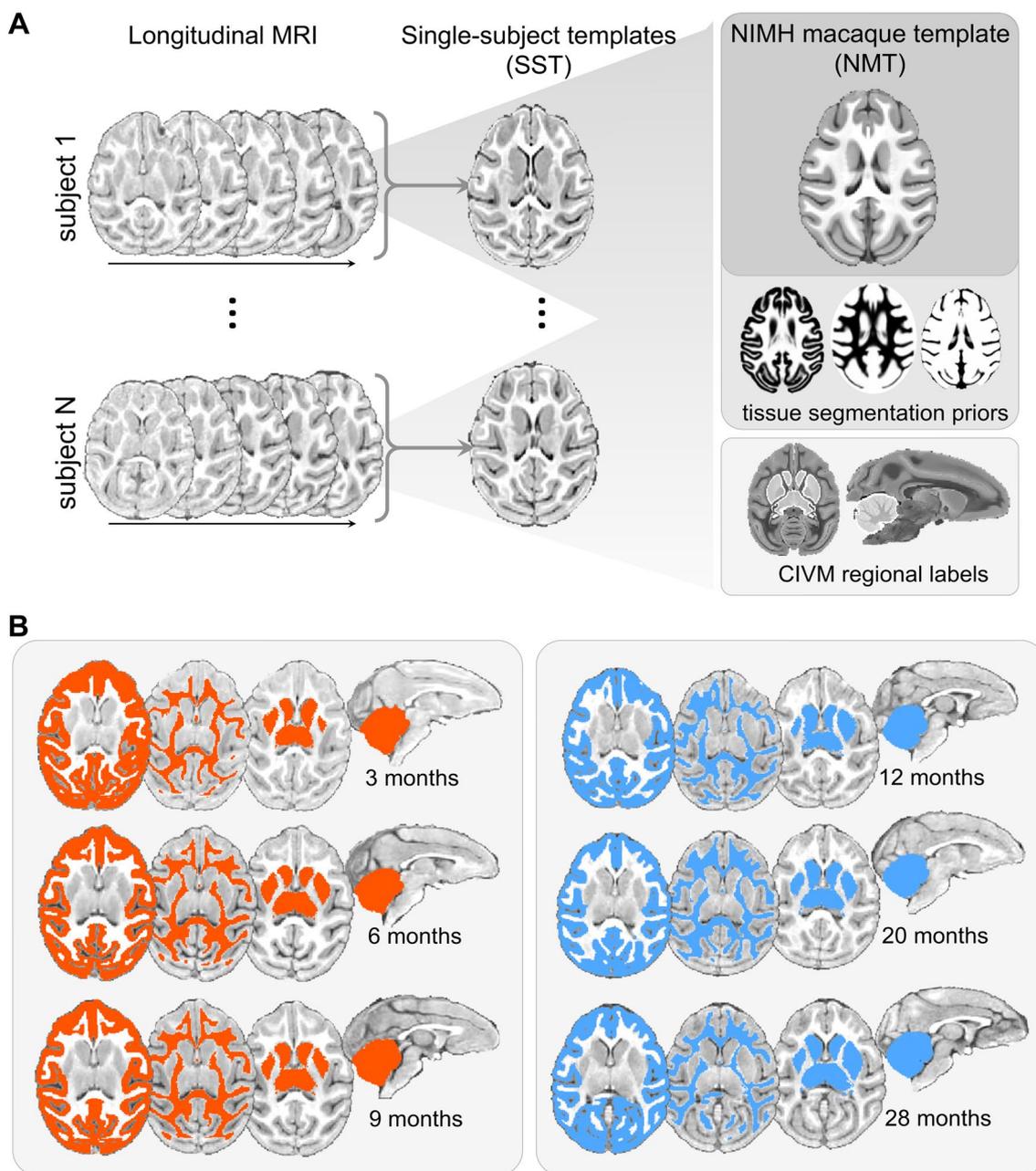
Fig. 2 Image processing pipeline and example tissue segmentations. **a** Longitudinal MRI scans were aligned to construct single-subject templates (SST) that were, in turn, aligned to a macaque template image. SST images were segmented using tissue priors from the NMT template, producing subject-specific tissue priors to initialise segmentation in each MRI image. Subcortical and cerebellar regions were labelled using the CIVM atlas. **b** Tissue segmentations are shown at three timepoints for two macaques (orange and blue)

necessary. The isointensity of different tissue classes in MRI of the early postnatal brain (Holland et al. 1986; Dietrich et al. 1988) can render tissue segmentation problematic (Weisenfeld and Warfield 2009) and prone to significant error. All T1 weighted scans acquired earlier than 3 months ($n = 12$) were excluded from further analysis due to largely failed tissue segmentation. A further three

timepoints were removed due to failed image registrations or tissue segmentations (Fig. 1).

Thus, for each timepoint ($n = 144$), we calculated volumes for the whole brain, cortical and subcortical grey matter, cerebral white matter and cerebellum for statistical analysis. As a secondary analysis, we examined regional variation of subcortical and allocortical structures separately, splitting

the subcortical grey matter mask into its constituent regions: thalamus, pallidum, striatum and the amygdalo-hippocampal formation.

Statistical analysis

We use Generalised Additive Models (GAMs) to model the relationship between brain tissue volume and age. Specifically, we can model the relationship between tissue volume, y, and age for n subjects as:

$$g(y) = f(\text{Age}) + \varepsilon,$$

where $f(\bullet)$ represents an unknown smooth function of age, $g(\bullet)$ represents a link function to map the distribution of the predicted values to that of the response and ε is an $n \times 1$ vector of errors, or residuals, assumed to be $i.i.d.$: $\varepsilon \in N\left(0, I\sigma_\varepsilon^2\right)$. In the case that y is normally distributed, $g(y) = y$.

This model can be extended to include multiple linear and nonlinear predictor variables, and when error is correlated across samples (i.e. with repeated measures of the same individual), by incorporating random effects to model the covariance between within-subject observations:

$$y = X\beta + \sum_{j=1}^{q} f_j(v_j) + Zb + \varepsilon,$$

where X is an m-observation $\times p$ matrix modelling p linear fixed effects, $\{v_1, \ldots, v_q\}$ is a set of q nonlinear predictors and Z is an $m \times (n \bullet r)$ design matrix modelling r random effects across n subjects. The linear parameters, β, and smooth functions, $f_{1 \ldots p}(\bullet)$, can then be estimated along with predictions of the random effects, b.

GAMs are flexible models that allow a data-driven estimation of nonlinear relationships between variables. As such, it is important to consider the risk of over-fitting to noise in the data during model estimation. In this study, we used the *mgcv* package (v1.8-22) implemented in R (v3.3.1) to model longitudinal tissue volume trajectories with GAMs. Smooth functions were estimated using penalised thin plate regression splines with automatic smoothness estimation maximising marginal likelihood (ML) (Wood 2003, 2011). These methods have been shown to robustly penalise over-fitting in finite samples and return less variable smoothing parameter estimates compared to alternative methods such as generalised cross-validation (Wood 2011).

To account for the longitudinal nature of the data, we included random effects to model subject-specific deviations from the group intercept or age relationship (random intercepts and slopes, respectively). We fit two mixed effects models for each tissue volume with fixed linear effects of sex and a smooth function of age as well as either random intercepts (*GAM1*), or both random intercepts and slopes (*GAM2*). For all tissue compartments, we also included a fixed linear effect of intracranial volume. For each tissue volume, we fit a separate model with the additional inclusion of an age:sex interaction effect for comparison. We compared the nonparametric GAM to a baseline linear mixed effects model with random intercepts using the *lme4* package (v1.1-15). Models were compared with the Akaike Information Criterion (AIC).

To test the contribution of each term to the final model for each tissue compartment, we fit a GAM including all terms and random effects and calculated the difference in explained variance excluding terms one at a time. Removal of terms that are important to the model fit will result in a larger reduction in variance explained. Wald tests were performed to test the significance of each parametric and smooth term's contribution to the model. Example analysis scripts are available at: https://github.com/DevelopmentalImagingMCRI.

Birth weight was available for 31 of 32 macaques (mean = 535.7 g, range: 425–672 g). To test associations between tissue volume and birth weight, we regressed individual predictions of random model effects (intercepts, and slopes when included in the model) onto birth weight for each tissue compartment.

Results

Intracranial volume

Longitudinal trajectories for intracranial volume are shown in Fig. 3. On average, ICV followed a nonlinear trajectory over time with an initial increase from 93.9 ml [95% C.I.: 91.5,96.2] ml at 3 months to 94.5 [92.2,96.7] ml at 5 months. This was followed by a small 2–3% decrease to approximately 92.9 [90.6,95.1] ml at 9 months and a slow, relatively stable increase of around 0.35 ml (0.37%) per month to reach 102.3 [98.2,106.3] ml at 36 months (Fig. 3).

A summary of model fits is shown in Table 1. Overall, the nonlinear models of ICV change produced a better fit of the data compared to a linear model. A Chi-squared test on the maximum-likelihood scores of the GAM models revealed a marginal improvement in the model fit when including both random intercepts and slopes ($\chi^2 = 2.86$, $p = 0.017$). However, the inclusion of random slopes only increased the variance explained by the model by $\sim 1.2\%$ (Table 3, $F_{15.9,31} = 279.6$, $p = 0.03$) and variation in the relationship between age and ICV was relatively low across subjects (Fig S1). Fixed effects parameters for the best-fit model (including intercepts and slopes) are shown in Table 2.

The inclusion of random intercepts resulted in an 11.8% increase in variance explained over other terms (Fig. 3c). Modelling age-related change in ICV between 3 and
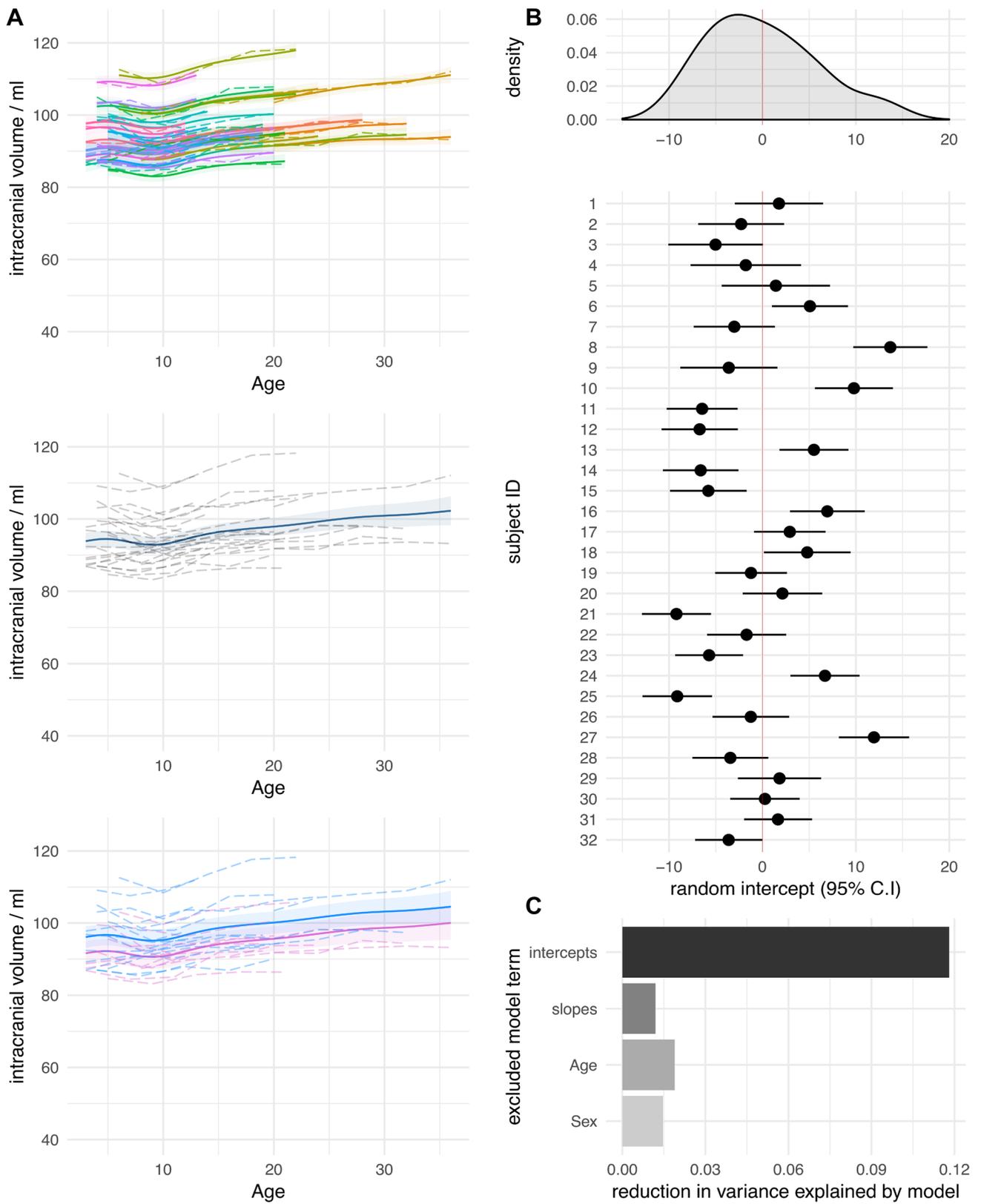
Fig. 3 Modelling longitudinal change in intracranial volume. **a** Modelled longitudinal trajectories are shown for all individuals (top row), the whole group (middle) and for males (blue) and females (pink) separately (bottom). Raw data are shown with dotted lines. Solid lines indicate predicted volume with 95% confidence intervals shaded. **b** The distribution of random intercepts (histogram, top) and prediction of individual random effects with 95% CI are shown. **c** Relative importance of models terms in the full model

Table 1 Model goodness-of-fit summaries

Model	Degrees-of-freedom	AIC
Intracranial volume		
Linear mixed model	5.00	725.48
GAM1: intercepts	41.61	587.71
GAM2: intercepts and slopes	58.32	558.88
Cortical grey matter		
Linear mixed model	6.00	617.08
GAM1: intercepts	41.35	456.06
GAM2: intercepts and slopes	41.35	456.06
White matter		
Linear mixed model	6.00	412.36
GAM1: intercepts	41.89	90.69
GAM2: intercepts and slopes	56.84	84.27
Subcortical grey matter		
Linear mixed model	6.00	− 28.79
GAM1: intercepts	37.03	− 167.96
GAM2: intercepts and slopes	51.51	− 203.61
Cerebellum		
Linear mixed model	6.00	9.06
GAM1: intercepts	36.90	− 84.47
GAM2: intercepts and slopes	46.39	− 95.13

36 months explained a moderate amount of variance in the data (~ 2%).

The distribution of predicted random intercepts for each subject is shown in Fig. 3b, and for random slopes in Fig S1. A large variation in head size was observed across the cohort. The group mean intercept [95% CI] was 93.53 ml [90.22, 96.83] (Table 2), in this case representing the mean ICV in females with individual ICV varying around this by ±15–20 ml. This variation is apparent in Fig. 3a (top row) where individual trajectories are overlaid on the volumetric data.

The inclusion of sex as a factor improved the variance explained by the model by around 1.5% (Fig. 3c). ICV was significantly larger in males than females by an average 4.5 ml [0.17, 8.82] ($p = 0.045$). Average male and female trajectories are shown in Fig. 3a (bottom row). Adding an additional model term to test whether the smooth function of age varied between sexes did not improve model fit (AIC with interaction effect: 583.9).

Cortical grey matter volume

On average, absolute CGM volume decreased rapidly from 52.9 [51.4, 54.4] ml at 3 months to 45.9 [44.6,47.2] ml at 9 months and remained relatively stable, reaching 46.7 [44.1,49.4] ml at 36 months. CGM volume was moderately greater in males than in females (mean = 2.42 ml [0.25, 4.60], $p = 0.03$; Fig S2).

Table 2 Parameter estimates for fixed linear effects in best-fit models

Term	Estimate	95% CI		Std. est	95% CI		p
		Lower	Upper		Lower	Upper	
Intracranial volume							
Intercept	93.53	90.22	96.83	–	–	–	–
Male	4.49	0.17	8.82	0.31	0.01	0.61	0.045
Cortical grey matter							
Intercept	− 3.73	− 6.48	2.01	–	–	–	–
Male	− 0.58	− 1.51	0.36	− 0.07	− 0.18	0.06	0.227
ICV	0.54	0.48	0.60	0.93	0.82	1.03	< 0.001
White matter							
Intercept	1.62	− 1.26	4.50	–	–	–	–
Male	0.82	− 0.02	1.65	0.13	− 0.004	0.27	0.06
ICV	0.15	0.12	0.18	0.42	0.28	0.42	< 0.001
Subcortical grey matter							
Intercept	1.34	0.51	2.17	–	–	–	–
Male	0.01	− 0.15	0.17	0.007	− 0.10	0.12	0.90
ICV	0.06	0.05	0.07	0.61	0.53	0.70	< 0.001
Cerebellum							
Intercept	2.59	1.45	3.72	–	–	–	–
Male	0.11	− 0.11	0.33	0.08	− 0.08	0.69	0.31
ICV	0.05	0.04	0.07	0.56	0.43	0.69	< 0.001

Fig. 4 Longitudinal trajectories of tissue volume compartments. Group average (top row) and male and female (middle row) trajectories are visualised as a proportion of ICV for **a** cortical grey matter, **b** white matter, **c** are shown with dotted lines, solid lines represent model fit with 95% CI shaded. Bottom row shows the reduction in variance explained when excluded model terms one-by-one from the full model fit. Trajectories for absolute volume are shown in Fig S2

As expected, CGM was largely dependent on ICV (Fig. 4a, bottom; Table 2). After correcting for linear scaling effects of ICV, cortical grey matter volume followed a nonlinear trajectory between 3 and 36 months. On average, cortical grey matter volume decreased, as a proportion of ICV, over the whole period (Fig. 4a, top). This trajectory was characterised by an initial period of decline between 3 and 8 months from 56.9% of ICV to 49.2% and a longer period of slower decrease, reaching an apparent plateau of around 45% by 30 months.

After accounting for variance due to individual differences in ICV, the inclusion of random intercepts significantly increased variance explained by the model (Table 3; $F_{24.3,30.0} = 5.18$, $p < 0.001$) but the inclusion of random slopes did not ($p = 0.556$). The best-fit model therefore included random intercepts only (Table 1). The inclusion of age (28%) or intracranial volume (23%) terms improved model fit significantly (Table 3; Fig. 4a, bottom) but there was no significant difference in relative cortical grey matter volume between sexes after accounting for ICV (Table 2; Fig. 4a, middle; $p = 0.23$).

White matter volume

Absolute WM volume increased from 11.9 [11.2, 12.6] ml at 3 months to a maximum of 20.4 [19.6, 21.2] ml at 36 months (Fig S2). On average, total WMV was greater in males than females by 0.8 ml, although this difference was not significant when including ICV in the full model (Table 2; Fig. 4b, middle).

White matter volume increased as a proportion of ICV over time from 12.5 to 19.9%, most rapidly over the first 7–8 months (Fig. 4b). Goodness-of-fit estimates are shown in Table 1. The inclusion of random slopes did not lead to a significantly better model fit over the inclusion of random intercepts alone ($\chi_2 = 0.87$, $p = 0.19$) and the inclusion of this term did not significantly increase the variance explained by the model (Table 3; Fig. 4b, bottom). In contrast, age and ICV accounted for relatively large improvements in variance explained by the model over other terms.

Cerebellar volume

Cerebellar volume increased from 7.0 [6.8, 7.2] ml (7.5% of ICV) at 3 months to 8.6 [8.3, 8.9] m (8.9%) at 36 months (Fig. 4c). Overall the inclusion of ICV (Table 2), age and random intercepts (Table 3) significantly increased explained variance (Fig. 3; all $p < 0.001$), with the best-fit model including random intercepts only (Table 1; $\chi_2 = 1.76$, $p = 0.06$). There was a significant effect of sex on absolute cerebellar volume ($\beta = 0.40$ [0.09, 0.72], $p = 0.014$), but not after including ICV in the full model (Table 2, $p = 0.31$).

Table 3 Significance of all smooth terms and random effects in mixed effects models

Term	Estimated dof*	Residual dof	F	p
Intracranial volume				
Intercepts	28.1	30.0	621.4	< 0.001
Slopes	15.5	31.0	279.6	0.027
S (age)	7.8	9.3	10.6	< 0.001
Cortical grey matter				
Intercepts	24.3	30.0	5.2	< 0.001
Slopes	0.0	31.0	0.0	0.556
S (age)	11.2	13.0	51.5	< 0.001
White matter				
Intercepts	28.0	30.0	279.8	< 0.001
Slopes	12.2	31.0	58.4	0.629
S (age)	8.3	9.9	214.1	< 0.001
Subcortical grey matter				
Intercepts	21.4	30.0	90.4	0.006
Slopes	19.9	31.0	75.9	0.006
S (age)	4.6	5.7	64.7	< 0.001
Cerebellum				
Intercepts	23.8	30.0	43.1	< 0.001
Slopes	11.4	31.0	18.7	0.111
S (age)	4.5	5.6	38.6	< 0.001

dof degrees-of-freedom

Subcortical and allocortical grey matter volume

Total subcortical grey matter volume increased from 6.4 [6.3, 6.6] ml to 8.4 [8.0, 8.7] ml between 3 and 36 months (Fig. 4d). There was no significant difference between males and females in absolute volume ($\beta = 0.27$ [−0.06, 0.60], $p = 0.112$). As a proportion of ICV, subcortical grey matter volume increased from 6.8 to 8.2% (Fig S3). The best-fit model included both random intercepts and slopes (Table 1; $\chi_2 = 8.20$, $p < 0.001$) and the inclusion of both random intercept and random slope terms independently increased the variance explained by the model (Table 3, both $p < 0.01$).

We performed a secondary analysis exploring regional trajectories in subcortical and allocortical growth. After correcting for ICV, we observed nonlinear increases in tissue volume in the thalamus (from 1.6 ml [1.7% ICV] at 3 months to 2.2 ml [2.2%] at 36 months), striatum (3.0 ml [3.2%] to 3.9 ml [3.7%]) and amygdalo-hippocampal region (1.4 ml [1.4%] to 1.7 ml [1.7%]), with the pallidum increasing linearly over the same time period (0.41 ml [0.04%] to 0.52 ml [0.05%]) (Table S3; Fig. 5).

There were no significant differences between males and females in any subcortical structure after correcting for ICV (Table S1), and no significant age:sex interactions. The best-fit models for each region are shown in Table S2. Best-fit
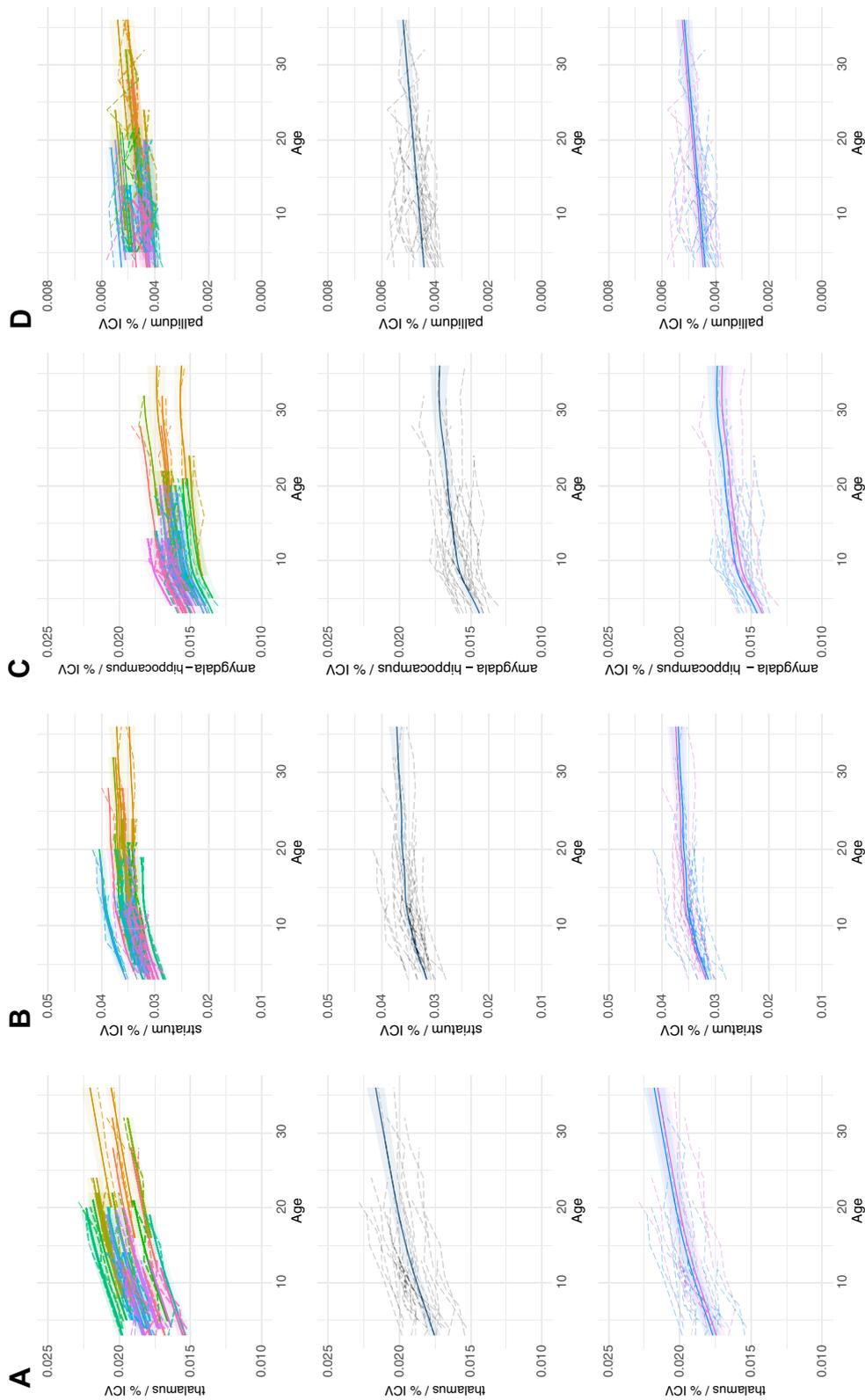
Fig. 5 Longitudinal trajectories of subcortical and allocortical structures. Group average trajectories are visualised as a proportion of ICV for the thalamus, striatum, pallidum and amygdalo-hippocampal complex. Data are shown for all individuals (top row), the whole group (middle) and for males (blue) and females (pink) separately (bottom row). Raw data are shown with dotted lines, solid lines represent model fit with 95% CI shaded

models included random intercepts only for the thalamus and pallidum, and random intercepts and slopes for the striatum ($\chi_2 = 6.71$, $p < 0.001$ compared to random intercepts only) and amygdalo-hippocampal region ($\chi_2 = 5.89$, $p < 0.001$). The extent of individual variation in predicted striatal and amygdalo-hippocampal volume across the full observation window for all subjects after accounting for the fixed effects of ICV and sex are shown in Figures S3 and S4, respectively.

Relating individual variations in tissue volume to birth weight

We found that lower birth weight was associated with lower total subcortical grey matter volume after accounting for ICV ($R^2 = 0.23$, $F = 8.78$, $p = 0.006$, $p < 0.05$ after FDR correction for multiple comparisons). Across all subcortical regions, birth weight was significantly associated with individual variation in striatal only with birth weight explaining 23% of the variance in predicted striatal volume model intercepts ($R^2 = 0.23$, $F = 8.41$, $p = 0.007$, $p < 0.05$ after FDR) and lower birth weights associated with lower striatal volumes. There were no other significant associations between birth weight and individual variation in volume (random intercepts) or rate of change of volume over time (random slopes) within subcortical and allocortical structures (all $p > 0.05$).

Individual variation in volume did not correlate with birth weight for ICV ($p = 0.40$), white matter ($p = 0.37$) or the cerebellum ($p = 0.22$). There was a small association between lower birth weight and higher relative cortical grey matter ($R^2 = 0.15$, $F = 4.92$, $p = 0.032$), though this did not survive correction for multiple comparisons. There were also no associations between birth weight and rate of change of volume over time (random slopes) for ICV ($p = 0.074$) or total subcortical grey matter ($p = 0.38$).

Discussion

In this paper, we present data-driven, nonlinear models of postnatal brain growth in the macaque across an age range broadly equivalent to 9 months to 9 years in humans. Intracranial volume significantly increased between 3 and 36 months. After accounting for changes in ICV over time, cortical grey matter decreased overall, whereas white matter, subcortical and allocortical grey matter and cerebellar volume all increased in volume. We also found that absolute intracranial volume varied significantly between individuals. After accounting for inter-individual differences in ICV, rate of change in cortical grey matter, white matter and cerebellar volume were relatively stable within the group, whereas rate of change of subcortical grey matter volume, specifically the striatum, amygdala and hippocampus varied significantly across subjects. Lower birth weight was not associated with

differences in ICV, but was significantly associated with lower striatal volume and moderately larger cortical grey matter volumes.

Intracranial volume, encompassing whole brain tissue as well as the ventricular system, increased by 9% between 3 and 36 months of age along a relatively stable, nonlinear trajectory with two notable deviations: an initial period of volume increase between 3 and 5 months followed by a period of slowed or decreasing volume between 5 and 9 months. This stalling in brain growth has been observed previously in the macaque brain. Scott et al. observed a transient plateau of brain growth between 26 and 39 weeks (approximately 6 to 9 months) in two smaller, independent cohorts ($n = 24$ and 21) with MRI acquired on different scanners (Scott et al. 2016). This was characterised by a lack of growth in male and negative growth in the female brain, along with a slowing in somatic growth during the same period. In this study, we observe a similar plateau, although we do not find significant evidence for different trajectories in male and female brain. In a smaller longitudinal cohort ($n = 7$), a similar pattern was reported, with decreasing brain volume observed in 4 out of 7 monkeys between 5 and 8 months that resulted in a group average decrease of 3% (Malkova et al. 2006). Here, we confirm these findings in a larger, developmental cohort.

While many neurodevelopmental processes are conserved across species, defining equivalent stages across species remains a complex task (Workman et al. 2013). Previous studies have approximated human age as equivalent to three times macaque age based on a comparison of lifespan and the age of pubertal maturation across species (Tigges et al. 1988; Chen et al. 2013). Based on this estimate, the period of slowed brain growth should fall between approximately 1 and 2 years of age in humans. Although few, longitudinal studies of infant brain development during this period have found that brain volume increases rapidly between birth and 1 year of age, doubling in size to reach 72% of adult volume. Between 1 and 2 years, growth rate decreases significantly with volume increasing by 15% over the second year (Knickmeyer et al. 2008). In a seminal study of brain weight, Dekaban and Sadowsky reported a dramatic slowing of growth rates by 3 years of age (Dekaban and Sadowsky 1978). In both studies, these patterns reflect changes in total brain tissue volume (i.e. parenchymal tissue, not including the ventricular system) and over the same period of time, the volume of the lateral ventricles was found to decrease by around 8% across the group (24% in males) (Knickmeyer et al. 2008). While this suggests that the observed decreases in ICV may be due to changes in ventricular volume rather than brain tissue, later work in a larger cohort estimated ventricular volume to increase around 18% between 1 and 2 years in humans (Knickmeyer et al. 2008; Gilmore et al. 2012). Alternative explanations may include a period of imbalance between progressive (axonal outgrowth, dendritic

arborisation) and regressive (synaptic pruning) neurodevelopmental processes that dramatically slow brain growth, or that decreases in brain volume are a direct consequence of decreased somatic growth (Passingham 1985; Bourgeois and Rakic 1993; Bourgeois et al. 1994; Scott et al. 2016).

From 10 months onwards, ICV was observed to increase slowly, gaining on average an additional 10% volume between 10 and 36 months (Fig. 3). In humans, early cross-sectional studies suggested the ICV peaks at around 10 years, approximately equivalent to 40 months in the macaque (Pfefferbaum et al. 1994). Longitudinal studies have since confirmed that ICV continues to increase steadily from mid-childhood before stabilising in adolescence, with an annual increase of around 1% reported (Giedd et al. 1999; Mills et al. 2016).

Using mixed effects models, we found significant inter-individual variation in ICV across the group. Brain volume at 3 months was predicted to vary by ± 15–20 ml around the group average. This represents substantial individual variation given that the average difference between male and female brains at the same age was estimated to be under 5 ml. No other differences were found between sexes across the other tissue compartments, after correcting for differences in ICV. This pattern highlights the importance of considering sample variation when comparing two or more populations. When considering neuroanatomical sex differences in humans, volumetric distributions are largely overlapping with relatively small mean difference (Ritchie et al. 2018). Similarly overlapping distributions have been reported in clinical populations including ADHD, autism and schizophrenia (Erp et al. 2016; Hoogman et al. 2017; van Rooij et al. 2018), highlighting the importance of longitudinal modelling to extract within-individual differences relative to the sample mean.

By comparison, cortical grey matter volume remained relatively stable over time. In absolute terms, CGM decreased by 13% between 3 and 9 months, before reaching a plateau by around 10 months. Histological evidence shows that thickness of the striate cortex is maximal at around 3 months of age, increasing by around 32% from thickness at birth (Bourgeois and Rakic 1993). In humans, Gilmore et al. reported an increase in total cortical grey matter of 107% between birth and 12 months (Gilmore et al. 2012). As such, it is likely that a significant increase in cortical grey matter is evident prior to 3 months in the macaques. However, segmentation of tissue compartments on MRI becomes difficult at younger ages due to the lack of contrast between grey and white matter on T1 and T2-weighted images (Holland et al. 1986; Dietrich et al. 1988). Tissue segmentations at this point rely heavily on manual tracing or specialised algorithms (de Macedo Rodrigues et al. 2015; Moeskops and Pluim 2017). In this study, we excluded scans acquired at less than 3 months due to errors in segmentation thus limiting our ability to define cortical development during this stage of development. Previous longitudinal studies in the macaque did not report grey matter volumes, instead estimating lobar volume inclusive of both white and grey matter (Scott et al. 2016), or manually traced volumes of white matter tissue alone (Malkova et al. 2006). In a cross-sectional study of macaques aged 10–64 months, total cortical grey matter remained stable across the observation window, as reported here (Knickmeyer et al. 2010).

While extant longitudinal data in humans are relatively sparse between 2 and 5 years of age, cortical grey matter is highest in childhood and appears to decline from age 5 onwards (Lebel and Beaulieu 2011; Mills et al. 2016). In our study, absolute cortical grey matter did not decline significantly with age after 10 months. However, cortical grey matter was significantly dependent on changes in intracranial volume and when ICV was included in the model, the effect of age on cortical grey matter followed a clear downward trajectory, mirroring that seen in humans when changes in ICV are taken into account (Mills et al. 2016). When visualised as a proportion of ICV, CGM decreased from an average of 57–45% (Fig. 4). After accounting for the substantial individual variation in ICV, the overall amount of cortical grey matter continued to vary across subjects, but the rate of change of cortical grey matter over time was relatively conserved. In humans, the rate of change in cortical grey matter volume varies significantly across cortical regions with developmental changes in higher-order association cortex occurring later than in sensorimotor regions (Giedd et al. 1999; Sowell et al. 2004; Gilmore et al. 2012) and similar patterns have been reported in macaques, even when total grey matter remains stable (Knickmeyer et al. 2010; Scott et al. 2016). This suggests that the amount of individual variability in cortical grey matter change may vary over regions and over time, and some aspect of this subject-level variation may be lost when considering the cortex as a whole.

White matter volume increased significantly over time both in absolute terms and as a proportion of ICV, with rapid expansion in the first 8 months and continued growth up to 36 months, confirming previous reports (Malkova et al. 2006). In humans, white matter continues to increase into mid-to-late adolescence (Lebel and Beaulieu 2011; Mills et al. 2016), and in macaques WM appears to peak post-puberty in young adulthood at approximately 4 years (Knickmeyer et al. 2010). This volumetric increase likely reflects the extent of ongoing myelination processes within the cerebral white matter. In humans, white matter myelination follows a protracted developmental course, extending into the second decade of life in humans (Yakovlev and Lecours 1967). Axonal myelination in non-human primates is more widespread at birth compared to humans and develops along a similar, though less prolonged, trajectory until adolescence (Malkova et al. 2006; Miller et al. 2012). After accounting

for variance due to ICV, we found that individual variation in white matter volume remained but, as with the cortical grey matter, rate of change of WM volume was relatively stable across subjects, suggesting that the neurobiological processes governing WM growth over time were relatively well-preserved across subjects.

In contrast, we found that subcortical and allocortical grey matter exhibited significant inter-individual variation in both volume and rate of change over time, even after accounting for individual differences in ICV. Cerebellar volume followed a similar trajectory to the subcortical grey matter, increasing rapidly over the first 8–9 months, however rate of change of cerebellar volume did not vary significantly across subjects. In humans, change in cerebellar and sub-cortical grey volume are strongly correlated in the second year of life (Knickmeyer et al. 2008), with cerebellar volume increasing until around 12–15 years (Tiemeier et al. 2010).

In humans, subcortical structures increase by around 106% over the first year of life, with rate of hippocampal growth notably slower (Gilmore et al. 2012). In later childhood, the thalamus, pallidum and hippocampus increase in volume into adolescence before decreasing, whereas caudate and putamen volumes decrease from around the age of 5 onwards (Herting et al. 2018). In macaques, manual tracing of the hippocampus reveal a similar trajectory to that described in humans, peaking by 3 years of age before declining slightly (Payne et al. 2010; Hunsaker et al. 2014). In contrast, using cross-sectional data, Knickmeyer described linear increases of caudate, putamen and hippocampal volume between 10 and 64 months in the macaque (Knickmeyer et al. 2010). In this cohort, variations in development of subcortical structures over time are shown in Fig. 5 after accounting for the effects of ICV. We observed a linear growth trajectory in the pallidum, but nonlinear increases in all other regions that mirrored the rate of change of the whole tissue volume. We also found significant individual variation in volume and rate of growth was evident in both the striatum and amygdala-hippocampal formation.

We found that lower birth weight was significantly associated with reduced subcortical volume, specifically in the striatum, after accounting for differences in ICV. Birth weight can be considered a sensitive marker of the intrauterine environment, reflecting somatic growth during gestation, and pathologically low birth weight in humans is associated with poor cognitive performance and adverse cerebral development in infancy and increased risk for neuropsychiatric disorder (Morsing et al. 2011; Sucksdorff et al. 2015; Ball et al. 2017). While birth weight in this cohort was within the normal range for macaques (Fujikura and Niemann 1967), in humans, normal birth weight variation has also been associated with differences in brain development and function in childhood (Raznahan et al. 2012). In typically developing children, normal variation in birth weight

is associated with caudate volume, after correcting for total brain volume (Walhovd et al. 2012), and in a longitudinal study of low birth weight adolescents, lower subcortical grey matter volumes were associated with higher rates of psychiatric symptoms between 15 and 19 years of age (Botellero et al. 2017). While the reported relationship is associative, we theorise that this correlation is a reflection of a putative relationship between aspects of the intrauterine environment and subcortical brain development although we are not able to exclude other postnatal influences from this relationship given the available data (Scott et al. 2016).

We also found a relatively small association between lower birth weight and increasing cortical grey matter volume (after correcting for ICV) between individuals. In humans, lower birth weight is associated with reductions in relative cortical volume at birth in humans (Tolsa et al. 2004) and, in typically developing children, increasing weight at birth is associated with specific increases in cortical area (Raznahan et al. 2012; Walhovd et al. 2012). In twins, after correction for intracranial volume, weak, negative associations between gestational age at birth and cortical grey matter volume have been reported (Soelen et al. 2010). Differences in cortical metrics may explain the observed discrepancies in reported here compared to previous human studies. Estimates of cortical volume capture information that relates to both area and thickness, and the contribution of each metric to measured volume may vary over the cortex, and there is substantial evidence that these constituent metrics of cortical volume are under differential developmental and genetic control (Winkler et al. 2018). Further exploration of cortical surface measures in this cohort is a promising avenue for future research. Improved cortical segmentation methods applicable to younger ages will also enable further exploration of the influence of pre- and postnatal environmental factors on brain development.

GAMs offer a powerful and flexible alternative to parametric modelling that do not require a priori specification of predictor functions. As such, regularised estimation of parameters that control the smoothness of the estimated functions is essential to avoid overfitting. Penalised thin plate regression splines represent a computationally efficient approach to fit regularised smooth functions and avoid undersmoothing (Wood 2011). In fitting these models, there is a concomitant risk of over smoothing that can in turn be mitigated in part through control and checking of the upper limit on the degrees of freedom associated with a smooth function (Wood 2017). Overall, the trajectories defined by our data-driven smooth tissue growth trajectories in approach reflect well previous observations of relatively the developing brain suggesting an appropriate model fit (Malkova et al. 2006; Scott et al. 2016).

In summary, we examined postnatal brain development in a densely sampled, longitudinal macaque cohort. We found

significant inter-individual differences in intracranial volume, and growth of subcortical grey matter regions. Future work will focus on the delineation of regional growth trajectories in the cortex: cortical grey matter regions likely have considerable spatial variation in developmental trajectories. The elucidation of individual regional cortical growth trajectories may provide further insight into early primate brain development.

Compliance with ethical standards

Conflict of interest The authors declare that they have no conflict of interest.

Ethical approval For the macaque data, the research protocol was approved by the local Institutional Animal Care and Use Committee at the University of Wisconsin-Madison. All applicable international, national, and/or institutional guidelines for the care and use of animals were followed. All procedures performed in studies involving animals were in accordance with the ethical standards of the institution or practice at which the studies were conducted.

References

Alexander-Bloch AF, Reiss PT, Rapoport J, McAdams H, Giedd JN, Bullmore ET, Gogtay N (2014) Abnormal cortical growth in schizophrenia targets normative modules of synchronized development. Biol Psychiatry 76:438–446

Amlien IK, Fjell AM, Tamnes CK, Grydeland H, Krogsrud SK, Chaplin TA, Rosa MGP, Walhovd KB (2016) Organizing principles of human cortical development—thickness and area from 4 to 30 years: insights from comparative primate neuroanatomy. Cereb Cortex 26:257–267

Aubert-Broche B, Fonov VS, García-Lorenzo D, Mouiha A, Guizard N, Coupé P, Eskildsen SF, Collins DL (2013) A new method for structural volume analysis of longitudinal brain MRI data and its application in studying the growth trajectories of anatomical brain structures in childhood. Neuroimage 82:393–402

Avants BB, Epstein CL, Grossman M, Gee JC (2008) Symmetric diffeomorphic image registration with cross-correlation: evaluating automated labeling of elderly and neurodegenerative brain. Med Image Anal 12:26–41

Avants BB, Tustison NJ, Song G, Cook PA, Klein A, Gee JC (2011a) A reproducible evaluation of ANTs similarity metric performance in brain image registration. Neuroimage 54:2033–2044

Avants BB, Tustison NJ, Wu J, Cook PA, Gee JC (2011b) An open source multivariate framework for *n*-tissue segmentation with evaluation on public data. Neuroinformatics 9:381–400

Bakken TE, Miller JA, Ding S-L, Sunkin SM, Smith KA, Ng L, Szafer A, Dalley RA, Royall JJ, Lemon T, Shapouri S, Aiona K, Arnold J, Bennett JL, Bertagnolli D, Bickley K, Boe A, Brouner K, Butler S, Byrnes E, Caldejon S, Carey A, Cate S, Chapin M, Chen J, Dee N, Desta T, Dolbeare TA, Dotson N, Ebbert A, Fulfs E, Gee G, Gilbert TL, Goldy J, Gourley L, Gregor B, Gu G, Hall J, Haradon Z, Haynor DR, Hejazinia N, Hoerder-Suabedissen A, Howard R, Jochim J, Kinnunen M, Kriedberg A, Kuan CL, Lau C, Lee C-K, Lee F, Luong L, Mastan N, May R, Melchor J, Mosqueda N, Mott E, Ngo K, Nyhus J, Oldre A, Olson E, Parente J, Parker PD, Parry S, Pendergraft J, Potekhina L, Reding M, Riley ZL, Roberts T, Rogers B, Roll K, Rosen D, Sandman D, Sarreal M, Shapovalova N, Shi S, Sjoquist N, Sodt AJ, Townsend R, Velasquez L, Wagley U, Wakeman WB, White C, Bennett C, Wu J, Young R, Youngstrom BL, Wohnoutka P, Gibbs RA, Rogers J, Hohmann JG, Hawrylycz MJ, Hevner RF, Molnár Z, Phillips JW, Dang C, Jones AR, Amaral DG, Bernard A, Lein ES (2016) A comprehensive transcriptional map of primate brain development. Nature 535:367–375

Ball G, Aljabar P, Nongena P, Kennea N, Gonzalez-Cinca N, Falconer S, Chew ATM, Harper N, Wurie J, Rutherford MA, Counsell SJ, Edwards AD (2017) Multimodal image analysis of clinical influences on preterm brain development. Ann Neurol 82:233–246

Botellero VL, Skranes J, Bjuland KJ, Håberg AK, Lydersen S, Brubakk A-M, Indredavik MS, Martinussen M (2017) A longitudinal study of associations between psychiatric symptoms and disorders and cerebral gray matter volumes in adolescents born very preterm. BMC Pediatrics 17:45

Bourgeois JP, Rakic P (1993) Changes of synaptic density in the primary visual cortex of the macaque monkey from fetal to adult stage. J Neurosci 13:2801–2820

Bourgeois JP, Goldman-Rakic PS, Rakic P (1994) Synaptogenesis in the prefrontal cortex of rhesus monkeys. Cereb Cortex 4:78–96

Calabrese E, Badea A, Coe CL, Lubach GR, Shi Y, Styner MA, Johnson GA (2015) A diffusion tensor MRI atlas of the postmortem rhesus macaque brain. NeuroImage 117:408–416

Chen X, Errangi B, Li L, Glasser MF, Westlye LT, Fjell AM, Walhovd KB, Hu X, Herndon JG, Preuss TM, Rilling JK (2013) Brain aging in humans, chimpanzees (Pan troglodytes), and rhesus macaques (Macaca mulatta): magnetic resonance imaging studies of macro- and micro-structural changes. Neurobiol Aging 34:2248–2260

Chiapponi C, Piras F, Fagioli S, Piras F, Caltagirone C, Spalletta G (2013) Age-related brain trajectories in schizophrenia: a systematic review of structural MRI studies. Psychiatry Res 214:83–93

Courchesne E, Carper R, Akshoomoff N (2003) Evidence of brain overgrowth in the first year of life in autism. JAMA 290:337–344

Cudeck R (1996) Mixed-effects models in the study of individual differences with repeated measures data. Multivar Behav Res 31:371–403

de Macedo Rodrigues K, Ben-Avi E, Sliva DD, Choe M-S, Drottar M, Wang R, Fischl B, Grant PE, Zöllei L (2015) A FreeSurfer-compliant consistent manual segmentation of infant brains spanning the 0–2 year age range. Front Hum Neurosci 9:21

Dekaban S (1978) Changes in brain weights during the span of human life: relation of brain weights to body heights and body weights. Ann Neurol 4:345–356

Dietrich R, Bradley W, Zaragoza E, Otto R, Taira R, Wilson G, Kangarloo H (1988) MR evaluation of early myelination patterns in normal and developmentally delayed infants. Am J Roentgenol 150:889–896

Douaud G, Mackay C, Andersson J, James S, Quested D, Ray MK, Connell J, Roberts N, Crow TJ, Matthews PM, Smith S, James A (2009) Schizophrenia delays and alters maturation of the brain in adolescence. Brain 132:2437–2448

Erp TGM van, Hibar DP, Rasmussen JM, Glahn DC, Pearlson GD, Andreassen OA, Agartz I, Westlye LT, Haukvik UK, Dale AM, Melle I, Hartberg CB, Gruber O, Kraemer B, Zilles D, Donohoe G, Kelly S, McDonald C, Morris DW, Cannon DM, Corvin A, Machielsen MWJ, Koenders L, Haan L de, Veltman DJ, Satterthwaite TD, Wolf DH, Gur RC, Gur RE, Potkin SG, Mathalon DH, Mueller BA, Preda A, Macciardi F, Ehrlich S, Walton E, Hass J, Calhoun VD, Bockholt HJ, Sponheim SR, Shoemaker JM, Haren NEM van, Pol HEH, Ophoff RA, Kahn RS, Roiz-Santiañez R, Crespo-Facorro B, Wang L, Alpert KI, Jönsson EG, Dimitrova R, Bois C, Whalley HC, McIntosh AM, Lawrie SM, Hashimoto R, Thompson PM, Turner JA (2016) Subcortical brain volume abnormalities in 2028 individuals with schizophrenia and 2540 healthy controls via the ENIGMA consortium. Mol Psychiatry 21:547–553

Foulkes L, Blakemore S-J (2018) Studying individual differences in human adolescent brain development. Nat Neurosci 21:315–323

Fujikura T, Niemann WH (1967) Birth weight, gestational age, and type of delivery in rhesus monkeys. Am J Obstet Gynecol 97:76–80

Gennatas ED, Avants BB, Wolf DH, Satterthwaite TD, Ruparel K, Ciric R, Hakonarson H, Gur RE, Gur RC (2017) Age-related effects and sex differences in gray matter density, volume, mass, and cortical thickness from childhood to young adulthood. J Neurosci 37:5065–5073

Giedd JN, Blumenthal J, Jeffries NO, Castellanos FX, Liu H, Zijdenbos A, Paus T, Evans AC, Rapoport JL (1999) Brain development during childhood and adolescence: a longitudinal MRI study. Nat Neurosci 2:861–863

Gilmore JH, Shi F, Woolson SL, Knickmeyer RC, Short SJ, Lin W, Zhu H, Hamer RM, Styner M, Shen D (2012) Longitudinal development of cortical and subcortical gray matter from birth to 2 years. Cereb Cortex 22:2478–2485

Grootel TJV, Meeson A, Munk MHJ, Kourtzi Z, Movshon JA, Logothetis NK, Kiorpes L (2017) Development of visual cortical function in infant macaques: A BOLD fMRI study. PLoS One 12:e0187942

Harvey PH, Pagel MD (1988) The allometric approach to species differences in brain size. Hum Evol 3:461–472

Hastie T, Tibshirani R (1986) Generalized additive models. Stat Sci 1:297–310

Hazlett HC, Gu H, Munsell BC, Kim SH, Styner M, Wolff JJ, Elison JT, Swanson MR, Zhu H, Botteron KN, Collins DL, Constantino JN, Dager SR, Estes AM, Evans AC, Fonov VS, Gerig G, Kostopoulos P, McKinstry RC, Pandey J, Paterson S, Pruett JR, Schultz RT, Shaw DW, Zwaigenbaum L, Piven J, The IBIS Network (2017) Early brain development in infants at high risk for autism spectrum disorder. Nature 542:348–351

Herculano-Houzel S, Manger PR, Kaas JH (2014) Brain scaling in mammalian evolution as a consequence of concerted and mosaic changes in numbers of neurons and average neuronal cell size. Front Neuroanat 8:77

Herting MM, Johnson C, Mills KL, Vijayakumar N, Dennison M, Liu C, Goddings A-L, Dahl RE, Sowell ER, Whittle S, Allen NB, Tamnes CK (2018) Development of subcortical volumes across adolescence in males and females: a multisample study of longitudinal changes. NeuroImage 172:194–205

Holland BA, Haas DK, Norman D, Brant-Zawadzki M, Newton TH (1986) MRI of normal brain maturation. Am J Neuroradiol 7:201–208

Holland D, Chang L, Ernst TM, Curran M, Buchthal SD, Alicata D, Skranes J, Johansen H, Hernandez A, Yamakawa R, Kuperman JM, Dale AM (2014) Structural growth trajectories and rates of change in the first 3 months of infant brain development. JAMA Neurol 71:1266–1274

Hoogman M, Bralten J, Hibar DP, Mennes M, Zwiers MP, Schweren LSJ, van Hulzen KJE, Medland SE, Shumskaya E, Jahanshad N, Zeeuw P de, Szekely E, Sudre G, Wolfers T, Onnink AMH, Dammers JT, Mostert JC, Vives-Gilabert Y, Kohls G, Oberwelland E, Seitz J, Schulte-Rüther M, Ambrosino S, Doyle AE, Høvik MF, Dramsdahl M, Tamm L, van Erp TGM, Dale A, Schork A, Conzelmann A, Zierhut K, Baur R, McCarthy H, Yoncheva YN, Cubillo A, Chantiluke K, Mehta MA, Paloyelis Y, Hohmann S, Baumeister S, Bramati I, Mattos P, Tovar-Moll F, Douglas P, Banaschewski T, Brandeis D, Kuntsi J, Asherson P, Rubia K, Kelly C, Martino AD, Milham MP, Castellanos FX, Frodl T, Zentis M, Lesch K-P, Reif A, Pauli P, Jernigan TL, Haavik J, Plessen KJ, Lundervold AJ, Hugdahl K, Seidman LJ, Biederman J, Rommelse N, Heslenfeld DJ, Hartman CA, Hoekstra PJ, Oosterlaan J, Polier G von, Konrad K, Vilarroya O, Ramos-Quiroga JA, Soliva JC, Durston S, Buitelaar JK, Faraone SV, Shaw P, Thompson PM, Franke B (2017) Subcortical brain volume differences in participants with attention deficit hyperactivity disorder in children and adults: a cross-sectional mega-analysis. Lancet Psychiatry 4:310–319

Hunsaker MR, Scott JA, Bauman MD, Schumann CM, Amaral DG (2014) Postnatal development of the hippocampus in the *Rhesus macaque* (Macaca mulatta): a longitudinal magnetic resonance imaging study. Hippocampus 24:794–807

Kanai R, Rees G (2011) The structural basis of inter-individual differences in human behaviour and cognition. Nat Rev Neurosci 12:231–242

King KM, Littlefield AK, McCabe CJ, Mills KL, Flournoy J, Chassin L (2017) Longitudinal modeling in developmental neuroimaging research: common challenges, and solutions from developmental psychology. Dev Cognit Neurosci 33:54–72

Kinney HC, Brody BA, Kloman AS, Gilles FH (1988) Sequence of central nervous system myelination in human infancy. II. Patterns of myelination in autopsied infants. J Neuropathol Exp Neurol 47:217–234

Knickmeyer RC, Styner M, Short SJ, Lubach GR, Kang C, Hamer R, Coe CL, Gilmore JH (2010) Maturational trajectories of cortical brain development through the pubertal transition: unique species and sex differences in the monkey revealed through structural magnetic resonance imaging. Cereb Cortex 20:1053–1063

Knickmeyer RC, Gouttard S, Kang C, Evans D, Wilber K, Smith JK, Hamer RM, Lin W, Gerig G, Gilmore JH. 2008. A Structural MRI study of human brain development from birth to 2 years. J Neurosci 28:12176–12182

Lampi KM, Lehtonen L, Tran PL, Suominen A, Lehti V, Banerjee PN, Gissler M, Brown AS, Sourander A (2012) Risk of autism spectrum disorders in low birth weight and small for gestational age infants. J Pediatr 161:830–836

Lebel C, Beaulieu C (2011) Longitudinal development of human brain wiring continues from childhood into adulthood. J Neurosci 31:10937–10947

Lenroot RK, Gogtay N, Greenstein DK, Wells EM, Wallace GL, Clasen LS, Blumenthal JD, Lerch J, Zijdenbos AP, Evans AC, Thompson PM, Giedd JN (2007) Sexual dimorphism of brain developmental trajectories during childhood and adolescence. NeuroImage 36:1065–1073

Madhyastha T, Peverill M, Koh N, McCabe C, Flournoy J, Mills K, King K, Pfeifer J, McLaughlin KA (2017) Current methods and

limitations for longitudinal fMRI analysis across development. Dev Cognit Neurosci 33:118–128

Malkova L, Heuer E, Saunders RC (2006) Longitudinal magnetic resonance imaging study of rhesus monkey brain development. Eur J Neurosci 24:3204–3212

Manjón JV, Coupé P, Buades A, Louis Collins D, Robles M (2012) New methods for MRI denoising based on sparseness and self-similarity. Med Image Anal 16:18–27

Miller DJ, Duka T, Stimpson CD, Schapiro SJ, Baze WB, McArthur MJ, Fobbs AJ, Sousa AMM, Šestan N, Wildman DE, Lipovich L, Kuzawa CW, Hof PR, Sherwood CC (2012) Prolonged myelination in human neocortical evolution. PNAS 109:16480–16485

Mills KL, Tamnes CK (2014) Methods and considerations for longitudinal structural brain imaging analysis across development. Dev Cognit Neurosci 9:172–190

Mills KL, Goddings A-L, Herting MM, Meuwese R, Blakemore S-J, Crone EA, Dahl RE, Güroğlu B, Raznahan A, Sowell ER, Tamnes CK (2016) Structural brain development between childhood and adulthood: convergence across four longitudinal samples. NeuroImage 141:273–281

Moeskops P, Pluim JPW (2017) Isointense infant brain MRI segmentation with a dilated convolutional neural network. arXiv :1708.02757

Morsing E, Åsard M, Ley D, Stjernqvist K, Maršál K (2011) Cognitive function after intrauterine growth restriction and very preterm birth. Pediatrics 127:e874–e882

Passingham RE (1985) Rates of brain development in mammals including man. BBE 26:167–175

Payne C, Machado CJ, Bliwise NG, Bachevalier J (2010) Maturation of the hippocampal formation and amygdala in macaca mulatta: a volumetric magnetic resonance imaging study. Hippocampus 20:922–935

Pfefferbaum A, Mathalon DH, Sullivan EV, Rawles JM, Zipursky RB, Lim KO (1994) A quantitative magnetic resonance imaging study of changes in brain morphology from infancy to late adulthood. Arch Neurol 51:874–887

Puelles L, Harrison M, Paxinos G, Watson C (2013) A developmental ontology for the mammalian brain based on the prosomeric model. Trends Neurosci 36:570–578

Raznahan A, Lerch JP, Lee N, Greenstein D, Wallace GL, Stockman M, Clasen L, Shaw PW, Giedd JN (2011) Patterns of coordinated anatomical change in human cortical development: a longitudinal neuroimaging study of maturational coupling. Neuron 72:873–884

Raznahan A, Greenstein D, Lee NR, Clasen LS, Giedd JN (2012) Prenatal growth in humans and postnatal brain maturation into late adolescence. PNAS 109:11366–11371

Raznahan A, Shaw PW, Lerch JP, Clasen LS, Greenstein D, Berman R, Pipitone J, Chakravarty MM, Giedd JN (2014) Longitudinal four-dimensional mapping of subcortical anatomy in human development. PNAS 111:1592–1597

Reuter M, Schmansky NJ, Rosas HD, Fischl B (2012) Within-subject template estimation for unbiased longitudinal image analysis. Neuroimage 61:1402–1418

Ritchie SJ, Cox SR, Shen X, Lombardo MV, Reus LM, Alloza C, Harris MA, Alderson HL, Hunter S, Neilson E, Liewald DCM, Auyeung B, Whalley HC, Lawrie SM, Gale CR, Bastin ME, McIntosh AM, Deary IJ (2018) Sex differences in the adult human brain: evidence from 5216 uk biobank participants. Cereb Cortex 28:2959–2975

Rogosa D, Brandt D, Zimowski M (1982) A growth curve approach to the measurement of change. Psychol Bull 92:726–748

Sakai T, Mikami A, Suzuki J, Miyabe-Nishiwaki T, Matsui M, Tomonaga M, Hamada Y, Matsuzawa T, Okano H, Oishi K (2017) Developmental trajectory of the corpus callosum from infancy to the juvenile stage: comparative MRI between chimpanzees and humans. PLoS One 12:e0179624

Scott JA, Grayson D, Fletcher E, Lee A, Bauman MD, Schumann CM, Buonocore MH, Amaral DG (2016) Longitudinal analysis of the developing rhesus monkey brain using magnetic resonance imaging: birth to adulthood. Brain Struct Funct 221:2847–2871

Seghier ML, Price CJ (2018) Interpreting and utilising intersubject variability in brain function. Trends Cognit Sci 22:517–530

Seidlitz J, Sponheim C, Glen D, Ye FQ, Saleem KS, Leopold DA, Ungerleider L, Messinger A (2018) A population MRI brain template and analysis tools for the macaque. Neuroimage 170:121–131

Shaw P, Eckstrand K, Sharp W, Blumenthal J, Lerch JP, Greenstein D, Clasen L, Evans A, Giedd J, Rapoport JL (2007) Attention-deficit/hyperactivity disorder is characterized by a delay in cortical maturation. Proc Natl Acad Sci USA 104:19649–19654

Smart IHM, Dehay C, Giroud P, Berland M, Kennedy H (2002) Unique morphological features of the proliferative zones and postmitotic compartments of the neural epithelium giving rise to striate and extrastriate cortex in the monkey. Cereb Cortex 12:37–53

Soelen ILC van, Brouwer RM, Peper JS, Beijsterveldt TCEM van, Leeuwen M van, Vries LS de, Kahn RS, Pol HEH, Boomsma DI (2010) Effects of gestational age and birth weight on brain volumes in healthy 9 year-old children. J Pediatr 156:896–901

Sowell ER, Thompson PM, Leonard CM, Welcome SE, Kan E, Toga AW (2004) Longitudinal mapping of cortical thickness and brain growth in normal children. J Neurosci 24:8223–8231

Sucksdorff M, Lehtonen L, Chudal R, Suominen A, Joelsson P, Gissler M, Sourander A (2015) Preterm birth and poor fetal growth as risk factors of attention-deficit/hyperactivity disorder. Pediatrics 136:e599–e608

Tamnes CK, Ostby Y, Fjell AM, Westlye LT, Due-Tønnessen P, Walhovd KB (2010) Brain maturation in adolescence and young adulthood: regional age-related changes in cortical thickness and white matter volume and microstructure. Cereb Cortex 20:534–548

Tamnes CK, Herting MM, Goddings A-L, Meuwese R, Blakemore S-J, Dahl RE, Güroğlu B, Raznahan A, Sowell ER, Crone EA, Mills KL (2017) Development of the cerebral cortex across adolescence: a multisample study of inter-related longitudinal changes in cortical volume, surface area, and thickness. J Neurosci 37:3402–3412

Tiemeier H, Lenroot RK, Greenstein DK, Tran L, Pierson R, Giedd JN (2010) Cerebellum development during childhood and adolescence: a longitudinal morphometric MRI study. Neuroimage 49:63–70

Tigges J, Gordon TP, McClure HM, Hall EC, Peters A (1988) Survival rate and life span of rhesus monkeys at the Yerkes regional primate research center. Am J Primatol 15:263–273

Tolsa CB, Zimine S, Warfield SK, Freschi M, Sancho Rossignol A, Lazeyras F, Hanquinet S, Pfizenmaier M, Huppi PS (2004) Early alteration of structural and functional brain development in premature infants born with intrauterine growth restriction. Pediatr Res 56:132–138

Tustison NJ, Avants BB, Cook PA, Zheng Y, Egan A, Yushkevich PA, Gee JC (2010) N4ITK: improved N3 bias correction. IEEE Trans Med Imaging 29:1310–1320

van Rooij D, Anagnostou E, Arango C, Auzias G, Behrmann M, Busatto GF, Calderoni S, Daly E, Deruelle C, Di Martino A, Dinstein I, Duran FLS, Durston S, Ecker C, Fair D, Fedor J, Fitzgerald J, Freitag CM, Gallagher L, Gori I, Haar S, Hoekstra L, Jahanshad N, Jalbrzikowski M, Janssen J, Lerch J, Luna B, Martinho MM, McGrath J, Muratori F, Murphy CM, Murphy DGM, O'Hearn K, Oranje B, Parellada M, Retico A, Rosa P, Rubia K, Shook D, Taylor M, Thompson PM, Tosetti M, Wallace GL, Zhou F, Buitelaar JK (2018) Cortical and subcortical brain morphometry differences between patients with autism spectrum disorder and healthy individuals across the lifespan: results from the ENIGMA ASD working group. Am J Psychiatry 175:359–369

Walhovd KB, Fjell AM, Brown TT, Kuperman JM, Chung Y, Hagler DJ, Roddey JC, Erhart M, McCabe C, Akshoomoff N, Amaral DG, Bloss CS, Libiger O, Schork NJ, Darst BF, Casey BJ, Chang L, Ernst TM, Frazier J, Gruen JR, Kaufmann WE, Murray SS, Zijl P van, Mostofsky S, Dale AM, for the Pediatric Imaging N (2012) Long-term influence of normal variation in neonatal characteristics on human brain development. PNAS 109:20089–20094

Walhovd KB, Fjell AM, Giedd J, Dale AM, Brown TT (2017) Through thick and thin: a need to reconcile contradictory results on trajectories in human cortical development. Cereb Cortex 27:1472–1481

Weisenfeld NI, Warfield SK (2009) Automatic segmentation of newborn brain MRI. Neuroimage 47:564–572

Wierenga L, Langen M, Ambrosino S, van Dijk S, Oranje B, Durston S (2014) Typical development of basal ganglia, hippocampus, amygdala and cerebellum from age 7 to 24. NeuroImage 96:67–72

Winkler AM, Greve DN, Bjuland KJ, Nichols TE, Sabuncu MR, Håberg AK, Skranes J, Rimol LM (2018) Joint analysis of cortical area and thickness as a replacement for the analysis of the volume of the cerebral cortex. Cereb Cortex 28:738–749

Wood SN (2003) Thin plate regression splines. J R Stat Soc 65:95–114

Wood SN (2011) Fast stable restricted maximum likelihood and marginal likelihood estimation of semiparametric generalized linear models. J R Stat Soc 73:3–36

Wood S (2017) Generalized additive models: an introduction with R. 2nd ed. CRC Press, Boca Raton

Workman AD, Charvet CJ, Clancy B, Darlington RB, Finlay BL (2013) Modeling transformations of neurodevelopmental sequences across mammalian species. J Neurosci 33:7368–7383

Yakovlev PI, Lecours AR (1967) The myelogenetic cycles of regional maturation of the brain. In: Minkowski A (ed) Regional development of the brain in early life. Blackwell, Oxford, pp 3–69

Young JT, Shi Y, Niethammer M, Grauer M, Coe CL, Lubach GR, Davis B, Budin F, Knickmeyer RC, Alexander AL, Styner MA (2017) The UNC-Wisconsin Rhesus Macaque neurodevelopment database: a structural MRI and DTI database of early postnatal development. Front Neurosci 11:29